3D LINE SEGMENT RECONSTRUCTION IN PIECEWISE PLANAR SCENES

Kai Li *Jian Yao*† *Menghan Xia* *Li Li*

School of Remote Sensing and Information Engineering, Wuhan University, P.R. China

† jian.yao@whu.edu.cn

ABSTRACT

This paper presents a new algorithm about 3D Line Segment (LS) reconstruction in piecewise planar scenes. Given a set of LS matches identified from two images, we first cluster them into groups that LS matches in each group are related by a same planar homography induced by a same space plane, which is subsequently estimated from the putatively reconstructed 3D LSs obtained by triangulating each pair of LS correspondences in the group. The final reconstructed 3D LSs are obtained by projecting the image LSs onto the estimated space plane. To reduce the incidence of the false grouping of LS matches, we formulate to solve the LS match grouping problem by solving a multi-label optimization problem via graph cuts. The advantages of our algorithm over others in this area are that it can generate satisfactory results using much fewer images and can recover the space planes where the reconstructed 3D LSs lie, which is beneficial for upper level applications.

Index Terms— 3D Line Segment Reconstruction, Piecewise Planar Scene Reconstruction, Graph Cuts.

1. INTRODUCTION

Feature point based 3D reconstruction methods [1, 2, 3, 4] might fail in man-made environments with a small number of distinctive interest points, e.g. urban and indoor scenes. In these environments, exploiting LSs extracted from images for 3D reconstruction can be an alternative way because LSs are often abundant in man-made scenes. Another benefit for exploiting LSs for 3D reconstruction is that we can obtain the wireframe of a scene with very few images and generate a recognizable model for the scene. This is because man-made objects (e.g. buildings) can often be outlined by a set of LSs. For example, to reconstruct the scene in Fig. 1(d), our proposed 3D LS reconstruction method can generate the 3D model shown in Fig. 1(e) using only two images. It is easy to recognize the scene from this 3D model, but hardly possible to achieve this from the extremely sparse point clouds obtained by some point based 3D reconstruction methods.

Despite of the above benefits for exploiting LSs for 3D reconstruction, it is often hard to reliably reconstruct 3D LSs because of the unstableness and low locating accuracy of extracted LSs. For example, to reconstruct the 3D LSs in the scene shown in Fig. 1(a), which can approximately be regarded to lie on a single space plane, when we used traditional way by triangulating the LS correspondences identified from two images, we obtained the 3D LSs shown in Fig 1(b). As we can see, many of the 3D LSs are reconstructed incorrectly. To solve this problem, some methods [5, 6, 7] resort to exploit multiple (three or more) images photographing a same scene to decrease the ambiguities and get more satisfactory results, which involves establishing LS correspondences between multiple images or some sophisticated hypothesizing-and-testing procedures.

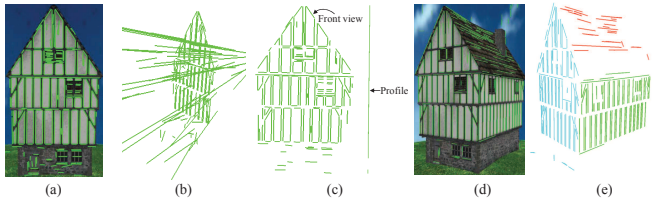

Fig. 1. An example of a problem in 3D line segment reconstruction and the results obtained by our proposed solution.

In this paper, we present a new solution to the aforementioned problem, which requires only two images. We first cluster LS matches identified from two images into groups that LS matches in each group are related by a same planar homogrpahy inducing by a single space plane, which is then estimated from the putatively reconstructed 3D LSs obtained by triangulating LS correspondences in this group. Once the space plane for a LS match group being estimated, the final 3D LSs can be obtained by projecting the LSs in one image onto the space plane. To reliably cluster LS match, we formulate to solve the LS match clustering problem by solving a multi-label optimization problem via graph cuts [8]. Fig. 1(c) shows our refined 3D LS reconstruction result for the scene shown in Fig. 1(a). As we can see, the problem existing in Fig. 1(b) is solved and the space plane in this scene is correctly recovered (the profile of the reconstructed 3D model turns out to be a line). Fig. 1(d) shows a scene comprised of multiple planes. Our method correctly reconstructs the 3D LSs, shown in Fig 1(e), using only two images and recovers the three main planes in the scene, with the correct clustering of the reconstructed 3D LSs w.r.t. the space planes they belong to. The contributions of this paper hence include the two aspects. First, we propose a new solution for solving the ambiguities in 3D LS reconstruction by LS match clustering and space plane estimation. Second, we propose to solve the LS match grouping problem by solving a multi-label optimization problem via graph cuts.

2. RELATED WORKS

We divide the existing 3D LS reconstruction methods into two categories: methods that require LS matching before the reconstruction procedure and those do not. Many methods in the former category focus on the exploitation of different mathematical representations for a 3D line to establish the projective relationship between a 2D line and its 3D correspondence, which is the foundation for 3D LS reconstruction and camera calibration based on lines. The projective relationship between 2D and 3D lines is not as explicitly as that the for points [9]. A series of representations for a line in 3D space have been proposed. They are plücker coordinates [10, 11, 12], pair of points [13, 14, 15, 16, 9], pair of planes [9], a unitary direction vector and a point on the line [17], the intersections with two orthogonal planes [18], and a more recent one, Cayley representa-

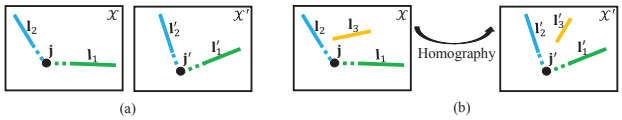

Fig. 2. An illustration of the principle ideas of the LS matching method presented in [25].

tion [19]. With these representations, researchers proposed various methods for reconstructing 3D lines and/or estimating the camera parameters. Some methods in the first category aim to reconstruct 3D LSs in certain scenes, like scenes meeting the Manhattan world assumption [20, 21], piecewise planar scenes [22] and poorly textured scenes [23]. The prior of these scenes helps decrease the uncertainties when reconstructing 3D LSs.

Some recent algorithms in this area attempt to free the reconstruction procedure from the heavy dependence on the LS matching procedure because it is hard to get reliable LS correspondences in some kinds of scenes, such as poorly textured indoor environments and scenes containing wiry structures (e.g. power pylons [6]). Most of these methods adopt the strategy to first generate a set of 3D hypotheses for each extracted LSs, either by sampling the depth of the endpoints of 3D LSs to camera centers [7], or triangulating putative LS correspondences after enforcing some soft constraints on the extract LSs [6, 5], and then to validate the hypotheses by projecting them back to images. In [24], a novel algorithm is proposed to obtain 3D LSs with an unknown global scale from a single image capturing a Manhattan world scene, which is possible because LSs on this special scene can only distribute in three orthogonal directions. This fact tremendously deceases the degrees of freedom when to reconstructed the scene LSs.

Our method belongs to the first category and the reconstruction procedure is based on our LS matching method presented in [25]. We focus only on obtaining 3D LSs, as well as recovering the main planes of piecewise planar scenes. The camera parameters are obtained by some external camera calibration methods. Unlike [22], which reconstructs 3D LSs in piecewise planar scenes using both feature points and LSs, our method exploits LSs only. The advantages of our algorithm over others in this area are that it can generate satisfactory results with much fewer images and can recover the space planes where the reconstructed 3D LSs lie, which is beneficial for upper level applications, such as scene understanding [26, 27] and building facade segmentation [22, 28, 29, 30].

3. ALGORITHM

3.1. Line Segment Matching

The proposed 3D LS reconstruction method is based on our LS matching method presented in [25], which provides some crucial input for the 3D LS reconstruction. We briefly summarize it here to help understand this paper. Refer to Fig. 2(a), suppose $\mathbf{l}_1$ and $\mathbf{l}_2$ are two LSs from the first image $\mathcal{X}$, and $\mathbf{l}'_1$ and $\mathbf{l}'_2$ from the second image $\mathcal{X}'$. The goal of LS matching is to establish the corresponding relationship between $\mathbf{l}_1$ and $\mathbf{l}'_1$, and $\mathbf{l}_2$ and $\mathbf{l}'_2$. For this aim, the LS matching method intersects $\mathbf{l}_1$ and $\mathbf{l}_2$, and $\mathbf{l}'_1$ and $\mathbf{l}'_2$, generating junction points $\mathbf{j}$ and $\mathbf{j}'$, respectively. Then, the method uses $\mathbf{j}$ and $\mathbf{j}'$ and the pairs of LSs forming them to construct two the so-called Line-Junction-Line (LJL) structures: ($\mathbf{l}_1$, $\mathbf{j}$, $\mathbf{l}_2$) and ($\mathbf{l}'_1$, $\mathbf{j}'$, $\mathbf{l}'_2$). To match the two LJLs, they are described by a robust descriptor, followed by some effective matching strategies. Once the two LJLs are successfully matched, two LS matches ($\mathbf{l}_1$, $\mathbf{l}'_1$) and ($\mathbf{l}_2$, $\mathbf{l}'_2$), and one point match ($\mathbf{j}$, $\mathbf{j}'$) can be obtained. The point matches obtained from all LJL matches found in the two images can be used to estimate the fundamental matrix $\mathbf{F}$ between the two images. The above strategy can only match LSs which lie near with other LSs because only spatially adjacent LSs are intersected to construct LJLs. For those LSs which lie far away from others and are not used to construct LJLs, they are matched by the local planar homographies computed from their neighboring LJL matches and the estimated $\mathbf{F}$. Please refer to [25] to know how to achieve this. For example, in Fig. 2(b), to match $\mathbf{l}_3$ and $\mathbf{l}'_3$, the proposed method finds their adjacent LJL match, ($\mathbf{l}_1$, $\mathbf{j}$, $\mathbf{l}_2$) and ($\mathbf{l}'_1$, $\mathbf{j}'$, $\mathbf{l}'_2$), and estimate a local planar homography using the LJL match and $\mathbf{F}$. Since the local homography can establish point-to-point correspondence, it can be used to map the endpoints of $\mathbf{l}_3$ to $\mathcal{X}'$, generating an estimated correspondence for $\mathbf{l}_3$, $\mathbf{l}^h_3$. If ($\mathbf{l}_3$, $\mathbf{l}'_3$) is a correct match, $\mathbf{l}^h_3$ must be very near to $\mathbf{l}'_3$. In this way, whether ($\mathbf{l}_3$, $\mathbf{l}'_3$) is a correct match can be determined.

LS matches and the local homographies estimated from some LS matches are used as input for the subsequent 3D LS reconstruction procedure.

3.2. Two-view Based 3D Line Segment Reconstruction

For two images, $\mathcal{X}$ and $\mathcal{X}'$, after matching the extracted LSs [15] from them using the above-presented method, we obtain a LS match set $\mathcal{M} = \{(\mathbf{l}_v, \mathbf{l}'_v)\}_{v=1}^{V}$, a homography matrix set $\mathcal{H} = \{\mathbf{H}_i\}_{i=1}^{I}$. Let the projection matrices for the two images be $\mathbf{P}$ and $\mathbf{P}'$. The 3D LS set corresponding to LS matches in $\mathcal{M}$ is $\mathcal{L} = \{\mathbf{L}_v\}_{v=1}^{V}$, which is obtained by triangulating the two LS correspondences in each match.

Line Segment Match Grouping The projections of space LSs from one space plane into two images would be related by a single homogrpahy. Based on this fact, we cluster the LS matches in $\mathcal{M}$ using the homography matrices in $\mathcal{H}$. For a LS match $(\mathbf{l}, \mathbf{l}') \in \mathcal{M}$, we find a homography matrix $\mathbf{H} \in \mathcal{H}$ which minimizes the distance of a pair of LSs according to a homography:

$$d = \mathbf{l}'^{\top}\mathbf{H}\mathbf{e}_1 + \mathbf{l}'^{\top}\mathbf{H}\mathbf{e}_2 + \mathbf{l}^{\top}\mathbf{H}^{-1}\mathbf{e}'_1 + \mathbf{l}^{\top}\mathbf{H}^{-1}\mathbf{e}'_2, \qquad (1)$$

where $\mathbf{e}_{i=1,2}$ and $\mathbf{e}'_{j=1,2}$ denote the two endpoints of $\mathbf{l}$ and $\mathbf{l}'$, respectively. After this, some homography matrices in $\mathcal{H}$ are assigned with some LS matches from $\mathcal{M}$, forming a LS match group set, $\mathcal{S} = \{\mathcal{G}_n\}_{n=1}^{N}$, where $\mathcal{G}_n$ denotes the n-th LS match group whose elements are from $\mathcal{M}$. Since LS matches in each group are clustered based on a same homography matrix induced by one space plane, their corresponding 3D LSs, $\mathcal{L}_s \subset \mathcal{L}$, are supposed to lie on the space plane. We can estimate the space plane from $\mathcal{L}_s$. But before that, we merge some groups in $\mathcal{S}$ to ensure LS matches induced by 3D LSs coming from a same space plane are clustered into only one group. For two LS match groups, $\mathcal{G}_i$ and $\mathcal{G}_j$, suppose they are formed based on the homographies, $\mathbf{H}_i$ and $\mathbf{H}_j$, respectively. If LS matches in $\mathcal{G}_i$ are consistent with $\mathbf{H}_j$, and vice versa, we merge the two groups into one. Here, a group of LS matches are *consistent* with a homography means the average of their distances according to the homography (defined in Eq. (1)) is a small value (2 pixels in this paper). After this, we obtain an updated LS group set $\mathcal{S}$.

Space Plane Estimation For a LS match group $\mathcal{G}_i \in \mathcal{S}$, all 3D LSs in its corresponding 3D LS set $\mathcal{L}_i \subset \mathcal{L}$ are supposed to lie on a single space plane. We estimate the space plane from the endpoints of the 3D LSs in $\mathcal{L}_i$ using RANSAC. Once the space plane being estimated, we can recompute the homography relating the LS matches in $\mathcal{G}_i$ and accept it only when the majority (0.8 in this paper) of the LS matches in $\mathcal{G}_i$ are consistent with it. After processing all elements in $\mathcal{S}$, we obtain a space plane set $\mathcal{P} = \{\mathbf{P}_m\}_{m=1}^{M}$, and the updated LS match group set $\mathcal{S} = \{\mathcal{G}_m\}_{m=1}^{M}$, whose elements correspond to the elements of $\mathcal{P}$.

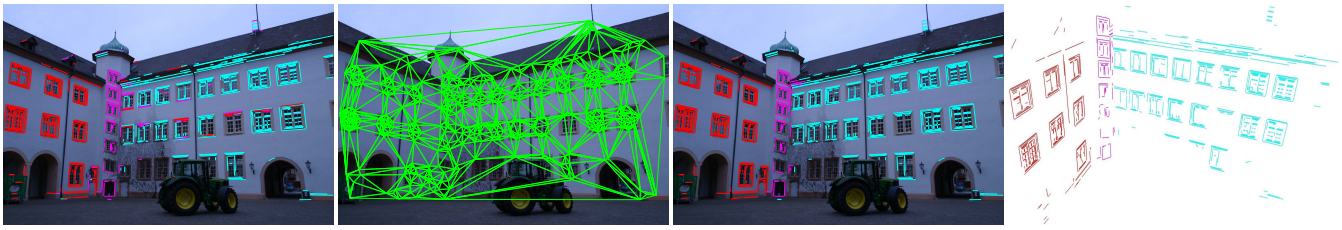

(a) (b) (c) (d)

Fig. 3. Some intermediate results generated by the proposed method based on two images.

Graph Cuts Based Line Segment Match Regrouping We found that it often brought in mistakes when we grouped LS matches only based on their distances according to estimated homographies that a LS match which is supposed to be assigned into one group but is clustered into another group mistakenly. This kinds of mistakes occur when there are several similar space planes in the scene and the estimated homographies are not so accurate, especially when the extracted LSs are not so precisely located. For instance, Fig. 3(a) shows an example of the LS match grouping result based on only the distances of the LS matches according to the estimated homographies. We draw in different colors the matched LSs in one of the two images to differentiate the groups to which they belong. The LSs drawn in the same color are supposed to appear on the same scene plane if they are correctly grouped. But, as we can see, a considerable number of the matched LSs are mistakenly clustered.

The spatial smoothness constraint on coplanar space LSs that they should be spatially adjacent with each other needs to be exploited for more reliably LS match grouping. To this aim, we propose to solve the LS match grouping problem by solving a multi-label optimization problem and through minimizing the following energy function to get the solution:

$$E = \sum_{p} D_p(l_p) + \sum_{p,q} V_{p,q}(l_p, l_q), \tag{2}$$

where the data term, D_p measures the cost of an object p being assigned with the label l_p, and the smoothness term, $V_{p,q}$ encourages a piecewise smooth labeling by assigning a cost whenever neighboring objects p and q being assigned with labels l_p and l_q, respectively. As for our problem, the data term D_p is the cost of a LS match $p = (\mathbf{l}_p, \mathbf{l}'_p)$ being labeled to belong to a group l_p, in which the homography relating the matches is assumed to be $\mathbf{H}_{l_p}$. Then, D_p can be calculated from Eq. (1). The smooth term $V_{p,q}$ measures the cost of two neighboring LS matches p and q being labeled to belong to groups l_p and l_q, respectively. We simply set it as a constant equaling 4 in pixels for all the labels. In this way, all terms in the objective function are defined. We resort to graph cuts to minimize the object function. We need to construct an adjacent graph to enable graph cuts to be exploited to solve our problem. Inspired by [31, 32], which constructed Delauney triangles for feature points, we construct Delauney triangles using the midpoints of matched LSs in one image to define the adjacent relationship between LS matches, as shown in Fig. 3(b). The weight for each edge in the adjacent graph is assigned by the Gaussian function according to the distance between the two vertices to encourage vertices with smaller distances being assigned with a same label in a higher possibility. The regrouping result corresponding the solution of the minimum of Eq. (2) is shown in Fig. 3(c). Comparing Figs. 3(a) and (c), we can observe that almost all mistakes have been corrected.

Once the falsely grouped LS matches are regrouped into correct groups, the final 3D LS corresponding to each match can be obtained simply by projecting one of the two LSs to its corresponding space plane. To remove the falsely reconstructed 3D LSs brought by few falsely grouped matches still existing after enforcing the smooth constraint. We intersect adjacent 3D planes and remove the 3D LSs that are beyond the intersection. After this, we obtain the final 3D LSs shown in Fig. 3(d). As we can see, the three main planes in this scene are correctly recovered and all 3D LSs are well reconstructed and correctly clustered w.r.t. the space planes on which they lie.

3.3. Multi-view Based 3D Line Segment Reconstruction

If more than two images are available, it is easy to extend the above two-view based 3D LS reconstruction method to deal with multiple views. We just need combine the results obtained from each pair of images. In details, we first reconstruct a set of space planes, $\mathcal{P}_1$, and the corresponding set of 3D LSs, $\mathcal{L}_1$ lying on these planes using the first two images. The two sets are used to initialize the overall space plane set, $\mathcal{P}_o = \mathcal{P}_1$, and the overall 3D LS set, $\mathcal{L}_o = \mathcal{L}_1$, for the whole scene. The subsequent images are used to refine the two initial overall sets. For each added image, it will be used to reconstruct 3D LSs with its previous one, generating a new space plane set, $\mathcal{P}_i$ and a new 3D LS set, $\mathcal{L}_i$. For a space plane $\mathbf{P}_i^j \in \mathcal{P}_i$, suppose its corresponding 3D LS set is $\mathcal{L}_i^j \in \mathcal{L}_i$, if it is consistent with a space plane $\mathbf{P}_o^m \in \mathcal{P}_o$, whose corresponding 3D LS set is $\mathcal{L}_o^m$, we merge $\mathbf{P}_i^j$ and $\mathbf{P}_o^m$ into a new space plane estimating from all 3D LSs in $\mathcal{L}_i^j$ and $\mathcal{L}_o^m$. 3D LSs in $\mathcal{L}_i^j$ and $\mathcal{L}_o^m$ are then projected onto the new space plane. Otherwise, we regard $\mathbf{P}_i^j$ as a new plane and update $\mathcal{P}_o$ and $\mathcal{L}_o$ as: $\mathcal{P}_o = \mathcal{P}_o \cup \{\mathbf{P}_i^j\}$ and $\mathcal{L}_o = \mathcal{L}_o \cup \mathcal{L}_i^j$. After processing all images, there would exist a considerable amount of duplications for 3D LSs in $\mathcal{L}_o$ because a same 3D LS can be visible in more than two views and be reconstructed in multiple times. We remove the duplications by keeping only one 3D LS for a group of ones which are spatially adjacent and have very similar directions [7].

4. EXPERIMENTS

We report in this section the experimental results of our method on a synthesis image dataset and a real image dataset.

Synthesis images The synthesis image dataset [7] has 80×3=240 images photographing around a CAD model from the upper, middle and bottom viewpoints. Each round consists of 80 images separated by a constant angle interval, 4.5°. An example image in the dataset is shown in Fig. 4(a). We employed for experiments only the 80 images for the middle round because we found in our initial experiments that the reconstruction result generated by our method based on the 80 images is negligibly different from that based on all 240 images, but the running time dropped significantly. Our reconstruction result is shown in Fig. 4(b). We can observe from this figure that the main planes in this scene are correctly recovered, and LSs on the scene are precisely represented in the reconstructed model and correctly clustered w.r.t. the planes to which they belong. We overlapped our result with the ground truth CAD model to qualitatively

(a) (b) (c) (d) (e)

Fig. 4. The 3D line segment reconstruction results of the proposed method on a synthesis image dataset.

	$\rho = 1.0$				$\rho = 0.6$			
	Ours	[7]	[6]	[5]	Ours	[7]	[6]	[5]
ME	0.083	0.162	0.065	–	0.076	0.137	0.044	0.029
RMSE	0.135	0.291	0.196	–	0.111	0.189	0.080	0.046

Table 1. The Mean Error (ME) and Root Mean Square Error (RMSE) data of the reconstruction results obtained by our method and several other ones on a synthesis dataset. "–" denotes that the corresponding measure data was not reported in the paper.

evaluate the reconstruction accuracy, as shown in Fig. 4(c). As we can see, the vast majority of the reconstructed LSs (in black) cling to or closely approach the ground truth model, indicating their high reconstruction accuracy. To quantitatively evaluate the reconstruction accuracy, following [7, 6, 5], we calculated the Hausdorff distances between densely sampled points along the 3D LSs and the ground truth CAD model, and computed the Mean Error (ME) and Root Mean Square Error (RMSE). Since we could not get the implementations of some state-of-the-art methods [7, 6, 5] in this area, we can only compare our measure data with that reported in the published papers, as shown in Table 1. It shows that when we set the cutoff distance threshold $\rho = 1.0$, as that applied in [6], the ME of our result is much better than [7], and only slightly inferior to [6]. But for the RMSE, our result is the best one. When we set $\rho = 0.6$ as that used in [5], our result is better than [7], but worse than both [6] and [5]. However, one fact that needs to be noticed is that both the ME and RMSE for our result increase slightly as ρ increases from 0.6 to 1.0, while they increase more significant for the others. It is a reasonable inference that if we increase ρ again, our method will be the best one among all these methods because our method has strong constraints for avoiding the emergence of gross outliers, but the others do not. Our 3D LSs are obtained by projecting image LSs to estimated space planes. If the space planes are correctly estimated, as for this scene, they will provide strong constraints for reconstructing 3D LSs. Once LS matches are correctly grouped, gross 3D LS outliers are unlikely to emerge. In fact, we found that when ρ is greater than 1.5, both ME and RMSE for our result remain unchanged and fix at 0.099 and 0.192, respectively. This indicates that all the sampled 3D points on the reconstructed 3D LSs have errors less than this threshold, and gross outliers do not exist.

The above experiment shows that our method can generate comparable results with others using one third of the images they used. In fact, our method can generate satisfactory result with even less images. Fig. 4(d) shows the 3D LS reconstruction result of the proposed method on 27 images obtained by taking one from every three images among the 80 images we used, and Fig. 4(e) shows the corresponding overlapping result between the reconstructed model and the ground truth model. We compare this model, referred as $\mathcal{M}_{27}$, with that generated from 80 images, referred as $\mathcal{M}_{80}$. Qualitatively speaking, there is no significant difference between $\mathcal{M}_{27}$ and $\mathcal{M}_{80}$, except some missing LSs on the roof and bottom of the captured house; the walls of the house are identically and completely reconstructed in both models. The great overlap between $\mathcal{M}_{27}$ and the ground truth model shown in Fig. 4(e) indicates that no gross outliers exist in this model, just the same as $\mathcal{M}_{80}$. Quantitatively speaking, the ME and RMSE for $\mathcal{M}_{27}$ are 0.068 and 0.098, respectively, when the cutoff threshold $\rho = 0.6$, and are 0.071 and 0.108, respectively, when $\rho = 1.0$. In both cases, the two measures for $\mathcal{M}_{27}$ are slightly better than those for $\mathcal{M}_{80}$. Moreover, same as $\mathcal{M}_{80}$, both ME and RMSE for $\mathcal{M}_{27}$ increase slightly with a greater ρ.

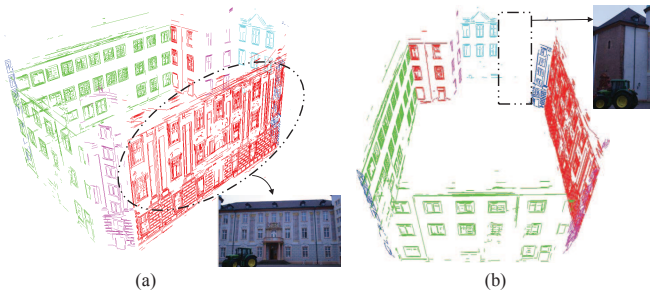

(a) (b)

Fig. 5. The 3D line segment reconstruction result of the proposed method on a real image dataset.

Real images The real image dataset [33] contains 30 images photographing a scene consisting of several houses. The reconstruction result is shown in Fig. 5. As we can see, the 3D LSs lying on the main planes of the scene are well reconstructed. The details of the scene are precisely presented in the reconstructed model, see the bricks and windows of the selected dashed elliptical region shown in Fig. 5(a). However, our method failed to reconstruct 3D LSs on the two main planes of this scene shown in the selected rectangle region in Fig. 5(b). This is because only several LSs are extracted on these two planes and even fewer LS matches are obtained. Our method is unable to reliably estimate a space plane when LS matches induced by 3D LSs on the plane are too few, and hence incapable to obtain the 3D LSs on it. The same reason also explains the missing on our model the representations of scene LSs on the roofs of the houses, and also the false reconstruction of the 3D LSs lying on the bottom of the house for the synthesis image dataset, as shown in Fig. 4(b). Incorporating point matches into space plane estimation seems a promising solution for this problem, as did in [22]. Solving this problem is our immediate future plan.

Running time The proposed 3D LS reconstruction method is easy to implement, and can be very efficient because it involves only some simple geometric operations of 2D and 3D LSs. The algorithm is currently implemented based on MATLAB. The unrefined codes took 32.2s on the synthesis dataset using 80 images and 52.2s on the real image dataset on a 3.4GHz Inter (R) Core(TM) processor with 12 GB of RAM.

5. CONCLUSIONS

We have presented in this paper a new algorithm about 3D LS reconstruction in piecewise planar scenes. A new solution is proposed to solve the uncertainties in 3D LS reconstruction by estimating space planes from clustered LS matches and projecting image LSs onto the space planes. To limit the incidence of the false clustering of LS matches, we propose to solve the LS match grouping problem by solving a multi-label optimization problem via graph cuts. Experiments on both synthesis and real image datasets verify the effectiveness of the proposed method and its superiority to others in this area for obtaining satisfactory results using much fewer images and reconstructing precise 3D LSs while recovering the space planes where they lie.

6. REFERENCES

[1] S. Agarwal, Y. Furukawa, N. Snavely, I. Simon, B. Curless, S. M. Seitz, and R. Szeliski. Building Rome in a day. *Communications of the ACM*, 54(10): 105-112, 2011.

[2] C. Wu. Towards linear-time incremental structure from motion. In *3DV*, 2011.

[3] Y. Furukawa and J. Ponce. Accurate, dense, and robust multiview stereopsis. *IEEE Transaction on Pattern Analysis and Machine Intelligence*, 32(8):1362-1376, 2010.

[4] N. Snavely, S. M. Seitz, and R. Szeliski. Photo tourism: exploring photo collections in 3D. *ACM Transactions on Graphics*, 25(3): 835-846, 2006.

[5] M. Hofer, M. Maurer, and H. Bischof. Improving sparse 3D models for man-made environments using line-based 3D reconstruction. In *3DV*, 2014.

[6] M. Hofer, A. Wendel, and H. Bischof. Incremental line-based 3D reconstruction using geometric constraints. In *BMVC*, 2013.

[7] A. Jain, C. Kurz, T. Thormahlen, and H. P. Seidel. Exploiting global connectivity constraints for reconstruction of 3D line segments from images. In *CVPR*, 2010.

[8] Y. Boykov, O. Veksler, and R. Zabih. Efficient approximate energy minimization via graph cuts. *IEEE Transaction on Pattern Analysis and Machine Intelligence*, 36(12), 1222-1239, 2001.

[9] R. Hartley and A. Zisserman. Multiple view geometry in computer vision. Cambridge university press, 2003.

[10] D. Matinec and T. Pajdla. Line reconstruction from many perspective images by factorization. In *CVPR*, 2003.

[11] B. Přibyl, P. Zemčík, and M. Čadík Camera pose estimation from lines using plücker coordinates. In *BMVC* 2015.

[12] A. Bartoli and P. Sturm. Structure-from-motion using lines: Representation, triangulation, and bundle adjustment. *Computer Vision and Image Understanding*, 100(3):416-441, 2005.

[13] P. Smith, I. D. Reid, and A. J. Davison. Real-time monocular SLAM with straight lines. In *BMVC* 2006.

[14] C. Baillard, C. Schmid, A. Zisserman, and A. Fitzgibbon. Automatic line matching and 3D reconstruction of buildings from multiple views. In *ISPRS Conference on Automatic Extraction of GIS Objects from Digital Imagery*, 1999.

[15] T. Werner and A. Zisserman. New techniques for automated architectural reconstruction from photographs In *ECCV*, 2002.

[16] A. F. Habib, M. Morgan, and Y. R. Lee Bundle adjustment with self-calibration using straight Lines. *The Photogrammetric Record*, 17(100), 635-650, 2002.

[17] C.J. Taylor and D.J. Kriegman Structure and motion from line segments in multiple images. *IEEE Transaction on Pattern Analysis and Machine Intelligence*, 17(11), 10211032, 1995.

[18] M. E. Spetsakis and J. Y. Aloimonos. Structure from motion using line correspondences. *International Journal of Computer Vision*, 4(3), 171-183, 1990.

[19] L. Zhang and R. Koch Structure and motion from line correspondences: representation, projection, initialization and sparse bundle adjustment. *Journal of Visual Communication and Image Representation*, 25(5), 904-915.

[20] G. Schindler, P. Krishnamurthy, and F. Dellaert. Line-based structure from motion for urban environments. In *3DPVT*, 2006.

[21] C. Kim and R. Manduchi Planar Structures from Line Correspondences in a Manhattan World. In *ACCV*, 2014.

[22] S. N. Sinha, D. Steedly, and R. Szeliski. Piecewise planar stereo for image-based rendering. In *ICCV*, 2009.

[23] H. Bay, A. Ess, A. Neubeck, and L. Van Gool. 3D from line segments in two poorly-textured, uncalibrated images. In *3DPVT*, 2006.

[24] S. Ramalingam and M. Brand. Lifting 3D Manhattan lines from a single image. In *ICCV*, 2013.

[25] K. Li, J. Yao, X. Lu, L. Li, and Z. Zhang. Hierarchical line matching based on line-junction-line structure descriptor and local homography estimation. doi:10.1016/j.neucom.2015.07.137, 2015.

[26] D. Hoiem, A. Efros, and M. Hebert. Closing the loop in scene interpretation. In Computer Vision and Pattern Recognition. In *CVPR*, 2008.

[27] J. Pan. Coherent Scene Understanding with 3D Geometric Reasoning. *Ph.D. Thesis, Carnegie Mellon University*, 2014.

[28] O. Teboul, L. Simon, P. Koutsourakis, and N. Paragios. Segmentation of building facades using procedural shape priors. In *CVPR*, 2010.

[29] J. A. Delmerico, P. David, and J. J. Corso. Building facade detection, segmentation, and parameter estimation for mobile robot stereo vision. *Image and Vision Computing*, 31(11), 841-852, 2013.

[30] J. Lee, Y. Lu, and D. Song. Planar building facade segmentation and mapping using appearance and geometric constraints. In *IROS*, 2014.

[31] A. Delong, A. Osokin, H. N. Isack, and Y. Boykov. Fast approximate energy minimization with label costs. *International Journal of Computer Vision*, 96(1), 1-27, 2012.

[32] T. T. Pham, T. J. Chin, J. Yu, and D. Suter. The random cluster model for robust geometric fitting. *IEEE Transaction on Pattern Analysis and Machine Intelligence*, 36(8), 1658-1671, 2014.

[33] C. Strecha, W. V Hansen, L. V. Gool, P. Fua, and U. Thoennessen. On benchmarking camera calibration and multi-view stereo for high resolution imagery. In *CVPR*, 2008.